Structure effects on electron-optical phonon interaction in GaAs/Al x Ga 1x As quantum wells

H. C. Lee, K. W. Sun, and C. P. Lee

Citation: Journal of Applied Physics **92**, 268 (2002); doi: 10.1063/1.1481963
View online: http://dx.doi.org/10.1063/1.1481963
View Table of Contents: http://scitation.aip.org/content/aip/journal/jap/92/1?ver=pdfcov
Published by the AIP Publishing

Structure effects on electron-optical phonon interaction in GaAs/$Al_xGa_{1-x}As$ quantum wells

H. C. Lee
Department of Electronic Engineering and Institute of Electronics, National Chiao Tung University, Hsinchu, Taiwan, Republic of China

K. W. Sun
Department of Physics, National Dong Hwa University, Hualien, Taiwan, Republic of China

C. P. Lee[a)]
Department of Electronic Engineering and Institute of Electronics, National Chiao Tung University, Hsinchu, Taiwan, Republic of China

(Received 4 January 2002; accepted for publication 5 April 2002)

Based on the dielectric continuum model, we have studied the electron-optical phonon scattering rates in GaAs/$Al_xGa_{1-x}As$ quantum wells with different structure parameters. It was found that the scattering rate of the symmetric interface phonon mode has a stronger dependence on the Al composition in the barriers than that of the confined mode. The effective phonon energy emitted by hot electrons in GaAs/$Al_xGa_{1-x}As$ quantum wells with various Al compositions was estimated and the calculated value agrees with the experimental results qualitatively. For the dependence on the well width, scattering rates of the $S+$ mode drop considerably as the well width is increased. The dependence of the electron-optical phonon interaction on structure parameters can be clearly explained by the *H* and *G* factors defined in the article. © *2002 American Institute of Physics.* [DOI: 10.1063/1.1481963]

I. INTRODUCTION

Electron-polar optical phonon interaction in III–V semiconductor quantum wells plays an important role for hot carrier relaxations, which influence the high-speed responses of many quantum devices. In the past, electron–phonon scattering rates in a quantum well were typically calculated using the bulk phonon model or the bulklike phonon model.[1–3] In the bulklike phonon model, the optical phonon modes are assumed to be the same as those in the bulk material while the electron wave functions incorporate quantum confinement. More recently, the dielectric continuum model[4–7] (DCM) and Huang–Zhu model[8] (HZM) were developed for dielectric slab problems and were more accurate than the bulk and the bulklike phonon models. The fundamental types of phonon modes[4,7,8] and the electron–phonon Hamiltonian[5,6,8] in heterostructures have become an interesting subject. Experimentally, Sood *et al.*[9,10] discovered the evidence of the confined longitudinal optical (LO), transverse optical (TO) phonons, and interface phonons in GaAs/AlAs superlattices using Raman scattering. An order of magnitude reduction in the intersubband scattering rates in GaAs/$Al_xGa_{1-x}As$ quantum wells was reported by Schlapp *et al.* using an infrared bleaching technique.[11] The reduced scattering rates were explained successfully by Jain and Das Sarma using the DCM[12] model.

In the last decade, techniques involving ultrafast spectroscopy became very powerful tools in studying carrier dynamics in semiconductors. Leo *et al.*[13,14] and Lobentanzer *et al.*[15] used time-resolved photoluminescence to study the hot carrier relaxation in a quasitwo-dimensional system. Their experimental results were analyzed with the average electron's energy-loss rate[16] (AELR) and indicated that the width of a quantum well had little effect on the hot carrier relaxation. However, the AELR in their analysis was calculated using the bulk phonon model.

More recently, a better method using the hot-electron neutral-acceptor luminescence[17] was developed to study the carrier relaxation mechanisms. It gives a better spectral resolution at lower carrier excitation densities than those of the ultrafast spectroscopy technique. This method has been used by Mirlin *et al.*,[18] Sapega *et al.*,[19] and Sun *et al.*[20] to determine the effective phonon energy in GaAs/$Al_xGa_{1-x}As$ quantum wells with various structure parameters. The effective phonon energy can be estimated in our calculations and be compared with experimental measurements.

The purpose of this article is to calculate the electron–phonon scattering rates in GaAs/$Al_xGa_{1-x}As$ quantum wells with various structure parameters based on the DCM model. Specifically, we focus on the dependence of the electron-optical phonon interaction on the Al composition in the barrier, which is the subject that is still lacking in earlier reports. The calculated results are compared with earlier experimental results.[20]

In the following content, we first describe the calculation methods and the assumptions made in this study. We then calculate the electron–phonon scattering rates with and without dynamical screening for all types of polar optical phonons based on the DCM model. The calculated effective

[a)]Author to whom correspondence should be addressed; present address: 1001 Ta Hsueh Road, Hsinchu, Taiwan; electronic mail: u8711819@cc.nctu.edu.tw

phonon energy is estimated and then compared with experimental results reported by Sun *et al.*[20]

II. THEORY

A. Phonon energy in GaAs/$Al_xGa_{1-x}As$ quantum wells

Base on DCM, there are six types of optical-phonon modes[6] in a dielectric slab. However, due to selection rules for the intrasubband scattering, only the confined LO mode, the half-space LO mode, and the symmetric interface modes were taken into consideration in our calculations. The confined phonons propagate in the well, and the component of the phonon wave vector along the layer growth direction (z direction) q_z is quantized. The half-space phonons, whose z component of the phonon wave vector is not restricted, propagate in the barrier. The symmetric interface phonons propagate along the interface, and the in-plane atomic displacement is symmetric with respect to the center of the well. The symmetric interface mode can be further divided into the symmetric plus branch (noted as $S+$ in the text), and the symmetric minus branch ($S-$). These two phonon branches also have different dispersion characteristics.

The energy of the $S+$ and the $S-$ interface phonon modes is given by the solution of

$$\varepsilon_1(\omega_{S\pm})\tanh(q_\parallel L/2)+\varepsilon_2(\omega_{S\pm})=0, \tag{1}$$

where the subscripts 1 and 2 denote GaAs and $Al_xGa_{1-x}As$, respectively, L is the well width, and $q_\parallel$ is the in-plane phonon wave vector. The lattice dielectric function is given by

$$\varepsilon_n(\omega_{S\pm})=\kappa_{\infty n}\frac{\omega_{S\pm}^2-\langle\omega_{Ln}\rangle^2}{\omega_{S\pm}^2-\langle\omega_{Tn}\rangle^2}, \tag{2}$$

where $\kappa_{\infty n}$ is the high-frequency relative permittivity of the nth layer. The optical phonon energy in the $Al_xGa_{1-x}As$ layer has two modes: the GaAslike mode and the AlAslike mode. $\langle\omega_{L1(T1)}\rangle$ represents the LO (TO) energy in the GaAs layer. $\langle\omega_{L2(T2)}\rangle$ represents the LO (TO) energy in the $Al_xGa_{1-x}As$ layer, and is taken as the average of those of the AlAslike mode $\omega_{L2(T2)}^{\mathrm{AlAs}}(x)$ and the GaAslike mode $\omega_{L2(T2)}^{\mathrm{GaAs}}(x)$

$$\langle\omega_{L2(T2)}\rangle=x\omega_{L2(T2)}^{\mathrm{AlAs}}(x)+(1-x)\omega_{L2(T2)}^{\mathrm{GaAs}}(x). \tag{3}$$

In our calculations, all parameters of the $Al_xGa_{1-x}As$ alloy were taken from the work of Adachi.[21]

In Fig. 1, we show the dependence of the phonon energy of the $S+$ mode and the $S-$ mode on the Al composition in the barrier at the minimum $q_{\parallel\min}$ and the maximum $q_{\parallel\max}$ in-plane phonon wave vectors with a well width of 5 nm. For the $S+$ mode, the phonon energy increases quickly with the Al composition for both $q_{\parallel\min}$ and $q_{\parallel\max}$. It approaches the LO phonon energy in the barrier layer when $q_\parallel$ approaches zero. The increase of the calculated $S+$ mode energy with Al composition at $q_{\parallel\min}$ agrees with the increased LO phonon energy in $Al_xGa_{1-x}As$ layer as Al composition is increased. For the $S-$ mode, the phonon energy has a weak dependence on the Al composition. It approaches the TO phonon energy of the well when $q_\parallel$ approaches zero. The weak dependence on the Al composition is easily understood because there is no Al in the well.

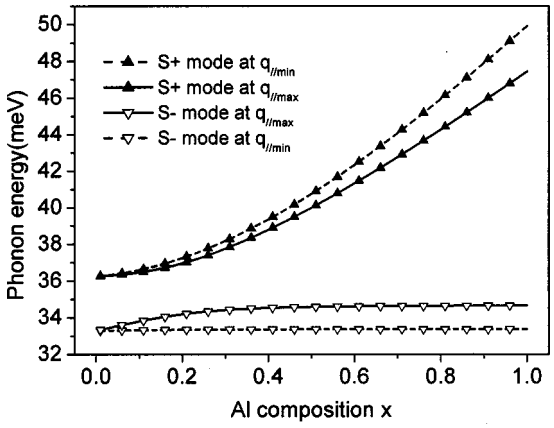

FIG. 1. The dependence of the phonon energy of the $S+$ mode and the $S-$ mode on the Al composition at $q_{\parallel\min}$ and $q_{\parallel\max}$.

B. Electron-optical phonon scattering rates with and without dynamical screening

Electron-optical phonon interaction Hamiltonians for all modes in a dielectric slab are taken from the work of Mori and Ando.[6] With the assumed average phonon energy in $Al_xGa_{1-x}As$ alloy shown in Eq. (3), intrasubband electron-optical phonon scattering rates in the lowest subband can be calculated using the Fermi's golden rule. The scattering rates are obtained by integrating over all possible states using the two-dimensional density of state function with states restricted by energy and momentum conservations. Scattering rates of the interface modes, $W_{S\pm}$, the confined mode, W_C, and the half-space mode, W_{HS}, are respectively written as

$$W_{S\pm}=\frac{e^2}{4\pi\varepsilon_0\hbar^3k}\sum_{n=1,2}\left\{m_n^*\int_{q_{\parallel\min}}^{q_{\parallel\max}}\frac{\omega_{S\pm}}{q_\parallel}[N(\omega_{S\pm})+1]\times|\langle\varphi_f|\phi_{S\pm}|\varphi_i\rangle|^2\left\{\left[h_1^{-1}(\omega_{S\pm})\tanh\left(\frac{1}{2}q_\parallel L\right)+h_2^{-1}(\omega_{S\pm})\right]\right\}^{-1}dq_\parallel\right\}, \tag{4}$$

$$W_C=\frac{m_1^*e^2\omega_C}{\pi^2\varepsilon_0\hbar^3k}\left(\frac{1}{\kappa_{\infty1}}-\frac{1}{\kappa_{01}}\right)[N(\omega_C)+1]\times\sum_p\frac{1}{p}\left\{|\langle\varphi_f|\phi_C|\varphi_i\rangle|^2\left[\tan^{-1}\left(\frac{q_{\parallel\max}L}{p\pi}\right)-\tan^{-1}\left(\frac{q_{\parallel\min}L}{p\pi}\right)\right]\right\}, \tag{5}$$

$$W_{\mathrm{HS}}=\frac{m_2^* e^2 \omega_{\mathrm{HS}}}{2\pi^2 \varepsilon_0 \hbar^3 k}\left(\frac{1}{\kappa_{\infty 2}}-\frac{1}{\kappa_{02}}\right)[N(\omega_{\mathrm{HS}})+1] \times \int_0^\infty \frac{1}{q_z}|\langle \varphi_f|\phi_{\mathrm{HS}}|\varphi_i\rangle|^2\left[\tan^{-1}\left(\frac{q_{\parallel \max}}{q_z}\right)-\tan^{-1}\left(\frac{q_{\parallel \min}}{q_z}\right)\right]dq_z, \tag{6}$$

where m_n^* is the effective mass of the electron, κ_{0n} is the static relative permittivity of the nth layer, and k is the wave vector of the electron $N(\omega_{S\pm})$, $N(\omega_C)$, and $N(\omega_{\mathrm{HS}})$ are phonon occupation numbers of the interface modes, the confined mode, and the half-space mode respectively. φ_i and φ_f are the wave functions of the electron of the initial and the final states in the quantum well. $\phi_{S\pm}$, ϕ_C, and ϕ_{HS}, given in Table I, are the potential functions of the interface, the confined, and the half-space modes respectively. The function, $h_n(\omega_{S\pm})$, is expressed as

$$h_n(\omega_{S\pm})=\left(\frac{1}{\kappa_{\infty n}}-\frac{1}{\kappa_{0n}}\right)\left(\frac{\langle \omega_{\mathrm{LO}n}\rangle^2}{\omega_{S\pm}^2}\right)\times\left(\frac{\omega_{S\pm}^2-\langle \omega_{\mathrm{TO}n}\rangle^2}{\langle \omega_{\mathrm{LO}n}\rangle^2-\langle \omega_{\mathrm{TO}n}\rangle^2}\right)^2. \tag{7}$$

TABLE I. The electric potential in a quantum well structure for the $S+$ mode, and the $S-$ mode, the confined mode, and the half-space mode.

	$z\leqslant -\frac{L}{2}$	$-\frac{L}{2}\leqslant z\leqslant \frac{L}{2}$	$z>\frac{L}{2}$
$\phi_{S\pm}$	$e^{q(z+L/2)}$	$\cosh(qz)/\cosh\left(q\frac{L}{2}\right)$	$e^{-q(z-L/2)}$
ϕ_c	0	$\cos\left(\frac{n\pi z}{L}\right)$	0
ϕ_{HS}	$\sin[q_z(z+\frac{1}{2}L)]$	0	$\sin[q_z(z-\frac{1}{2}L)]$

In order to clearly explain the dependence of scattering rates on the structure parameters for the interface modes, we introduce the H factor, defined as

$$H=\left[h_1^{-1}(\omega_{S\pm})\tanh\left(\frac{1}{2}q_{\parallel}L\right)+h_2^{-1}(\omega_{S\pm})\right]^{-1}. \tag{8}$$

It appears in the scattering rate equation [Eq. (4)] for the interface modes. In addition, we call the overlap integral, $\langle \varphi_f|\phi|\varphi_i\rangle$, for the electric potential G factors for the phonon modes. For $S+$ and $S-$ modes, the G factor in the well is

$$G_{S\pm}^w=\frac{1}{\cosh(1/2\,q_{\parallel}L)}\cdot\frac{2}{[\hbar/\sqrt{2m_2(\Delta E_C-E_1)}][1+\cos[(\sqrt{2m_1E_1}/\hbar)L]]+L+(\hbar/\sqrt{2m_1E_1})\sin[(\sqrt{2m_1E_1}/\hbar)L]} \cdot\left[\frac{1}{q_{\parallel}}\sinh\left(\frac{1}{2}q_{\parallel}L\right)+\frac{q_{\parallel}\sinh(1/2\,q_{\parallel}L)\cos[(\sqrt{2m_1E_1}/\hbar)L]+2(\sqrt{2m_1E_1}/\hbar)\cosh(1/2\,q_{\parallel}L)\sin[(\sqrt{2m_1E_1}/\hbar)L]}{q_{\parallel}^2+(8m_1E_1/\hbar^2)}\right]. \tag{9}$$

In the barrier, it is

$$G_{S\pm}^b=\frac{4}{q_{\parallel}+[\sqrt{8m_2(\Delta E_C-E_1)}/\hbar]} \cdot\frac{\cos^2[(\sqrt{2m_1E_1}/2\hbar)L]}{[\hbar/\sqrt{2m_2(\Delta E_C-E_1)}]\{1+\cos(\sqrt{2m_1E_1}/\hbar)L]\}+L+(\hbar/\sqrt{2m_1E_1})\sin[(\sqrt{2m_1E_1}/\hbar)L]}, \tag{10}$$

For the confined mode, the G factor of the pth mode is

$$G_C^p=\frac{L}{\pi}+\frac{1}{2}\left\{\frac{\sin\{[(p\pi/L)-(\sqrt{8m_1E_1}/\hbar)](L/2)\}}{(p\pi/L)-(\sqrt{8m_1E_1}/\hbar)}+\frac{\sin\{[(p\pi/L)+(\sqrt{8m_1E_1}/\hbar)](L/2\}}{(p\pi/L)+(\sqrt{8m_1E_1}/\hbar)}\right\},\quad p=1,3,5\ldots \tag{11}$$

$$G_C^p=0,\quad p=2,4,6\ldots \tag{12}$$

For the half-space mode, it is

$$G_{\mathrm{HS}}=\frac{4\cos^2[(\sqrt{2m_1E_1}/2\hbar)L]}{[\hbar/\sqrt{2m_2(\Delta E_C-E_1)}]\{1+\cos[(\sqrt{2m_1E_1}/\hbar)L]\}+L+(\hbar/\sqrt{2m_1E_1})\sin[(\sqrt{2m_1E_1}/\hbar)L]} \cdot\frac{q_z}{[8m_2(\Delta E_C-E_1)/\hbar^2]+q_z^2}, \tag{13}$$

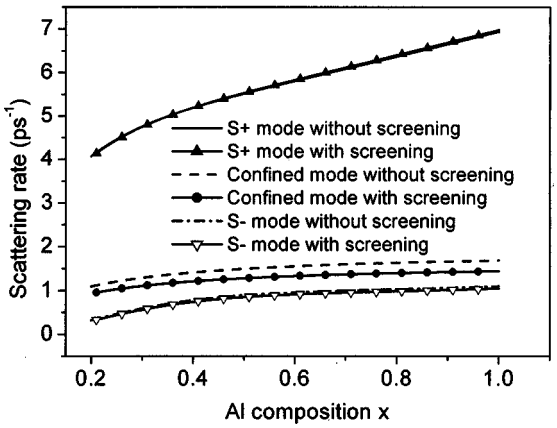

FIG. 2. The dependence of the electron–phonon scattering rate of the $S+$ mode, the confined mode, and the $S-$ mode on the Al composition. The well width is 5 nm, the lattice temperature is 15 K, and the amount of the excess kinetic energy of the electron is 50 meV.

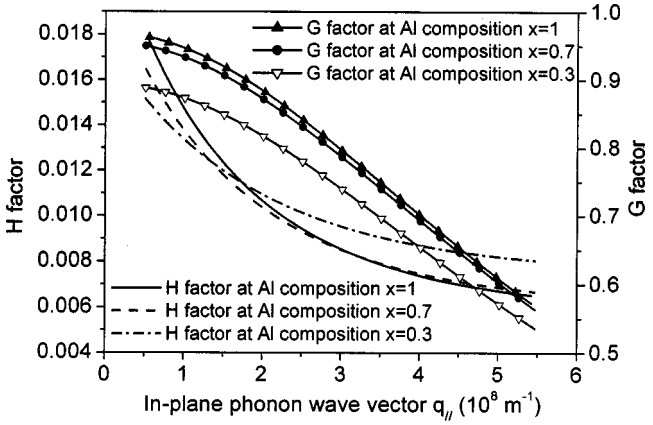

FIG. 3. The dependence of the H factor and the G factor for the $S+$ mode on $q_{\parallel}$ at three Al compositions in the barrier, 0.3, 0.7, and 1.

where E_1 is the ground-state energy, and ΔE_C is the barrier height of the quantum well.

We used the DCM instead of the HZM[8] for the treatment of the boundaries. It is because the scattering rate calculated by HZM gives an unreasonably large scattering rate even with very narrow well width due to the slow convergence of the modes of the higher order.

Dynamical screening in electron–phonon interaction is treated by random phase approximation, and the two-dimensional longitudinal dielectric function of plasma[22] is given by

$$\varepsilon(q,\omega)=1-V_q\Pi_0(q,\omega), \tag{14}$$

where $V_q=e^2/2\varepsilon_0\kappa_{\infty n}q$ is the two-dimensional Fourier transform of the Coulomb interaction, and $\Pi_0(q,\omega)=-(n_{2D}/E_F)(k_F/q)[(q/k_F)-(a_+^2-1)^{1/2}+(a_-^2-1)^{1/2}]$ is the zero-temperature polarizability function, where n_{2D} is the sheet charge density, k_F is Fermi wave vector, E_F is Fermi energy, and $a_{\pm}=\dfrac{\omega+i\gamma}{qv_F}\pm\dfrac{q}{2k_F}$. ω is the phonon energy, damping coefficient[23] $\gamma=(0.2-0.3)\omega$, and v_F is the Fermi velocity.

III. RESULTS AND DISCUSSION

In our calculations, band-offset ratio $\Delta E_c:\Delta E_v$ in $GaAs/Al_xGa_{1-x}As$ quantum wells was chosen to be 65:35. The electrons were given an excess energy of 50 meV so that the intersubband transition can be neglected. The sheet-charge density was chosen to be 5×10^{10} cm^{-2}.

In Fig. 2, we show the calculated dependence of electron-optical phonon scattering rates on the Al composition for various types of phonon modes in a 5 nm wide $GaAs/Al_xGa_{1-x}As$ quantum well with a lattice temperature of 15 K. For the $S+$ mode, the scattering rate increases from 4.1 to 6.9 ps^{-1} as the Al composition, x, is increased from 0.2 to 1. In order to interpret the results, we show in Fig. 3 the dependence of the H factor and the G factor on $q_{\parallel}$. As we can see, both the H factor and the G factor increase with the Al composition at small $q_{\parallel}$. Since the $S+$ mode favors the small-angle scattering, this dependence follows the behavior of the H and the G factors at small $q_{\parallel}$. For the $S-$ mode, the scattering rate increases from 0.32 to 1.1 ps^{-1} as the Al composition is increased from 0.2 to 1. The strong dependence on the Al composition is mostly due to the H factor. In Fig. 4, we show the dependence of the H factor on $q_{\parallel}$. As $q_{\parallel}$ decreases toward zero, ω_{S-} approaches the TO phonon energy in the well. This leads to the decrease of the H factor. Because of this, the small-angle scattering for the $S-$ mode is not as important as that for other phonon modes. In Fig. 2, we have also found that the screening effect for the $S+$ mode and the $S-$ mode is not significant.

Comparing to the $S+$ and the $S-$ modes, the scattering rate of the confined phonon mode does not show strong dependence with the Al composition in the range that we have investigated. It is because that the G factor in the expression of the scattering rate equation for the confined phonon mode is less sensitive to the Al composition. The screening effect for the confined mode is stronger than that of the $S+$ and the $S-$ interface modes.

For the 5 nm well, the electron wave function does not penetrate deep into the barriers. Therefore, the contribution of the half-space mode to the scattering rate is insignificant

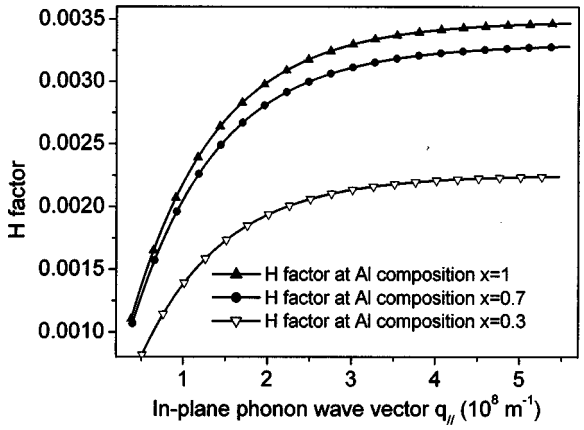

FIG. 4. The dependence of the H factor for the $S-$ mode on $q_{\parallel}$ at three Al compositions in the barrier, 0.3, 0.7, and 1.

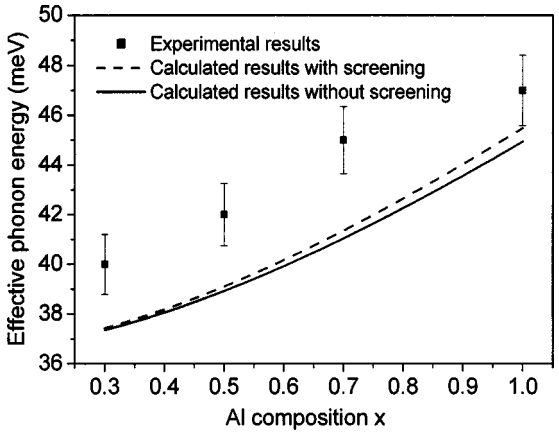

FIG. 5. The comparison of experimental results and calculated results for the dependence of the effective phonon energy on the Al composition. The well width is 5 nm, the lattice temperature is 15 K, and the amount of the excess kinetic energy of the electron is 180 meV.

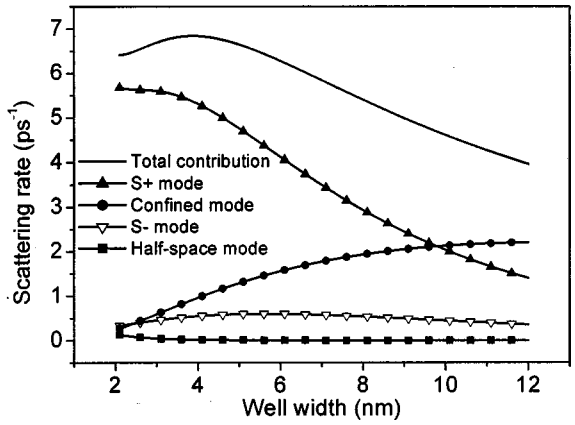

FIG. 6. The dependence of the electron-optical phonon scattering rate of the $S+$ mode, the confined mode, the $S-$ mode, the half-space mode, and the total rate contributed by all types of phonon modes on the well width. The Al composition is 0.3, the lattice temperature is 15 K, and the amount of the excess kinetic energy of the electron is 50 meV.

in comparing to the other three types of phonon modes and is not considered here.

The calculated results were compared with the experimental results[20] performed by hot electron neutral-acceptor luminescence for GaAs/$Al_xGa_{1-x}As$ quantum wells with various Al compositions. The calculated effective phonon energy (ω_{eff}) is given by

$$\omega_{\text{eff}}=\frac{W_{S+}\omega_{S+}+W_{S-}\omega_{S-}+W_C\omega_C}{W_{S+}+W_{S-}+W_C}. \tag{15}$$

In Fig. 5, we show the dependence of the effective phonon energy on the Al composition of both the experimental result[20] and our calculations. There are two calculated curves in Fig. 5. The solid line represents the results without screening and the dash one with screening. Since the $S+$ mode plays the dominant role in the calculated scattering rate among all phonon modes, the calculated effective phonon energy basically follows the behavior of the $S+$ mode. The tendency of the calculations is in good agreement with the experiments.

The minor difference between the measured result and the calculated result on the effective phonon energy is attributed to the assumptions that we made in the calculations of the average phonon energy in $Al_xGa_{1-x}As$ alloy, which probably simplified the complexity of the phonon spectrum in the ternary compound.

In Fig. 6, we show the dependence of scattering rates on the well width for various types of phonon modes with an Al composition $x=0.3$ in the barriers. Other parameters are kept the same as in previous calculations. For the $S+$ mode, the scattering rate decreases considerably from 5.3 to 1.4 ps^{-1} as the well width is increased from 4 to 12 nm. We attribute this to the decrease of the H factor and the G factor as the well width is increased. When the wells move toward wider wells, the electron wave functions centered at the middle of the well do not spread deep into the interfaces as in the narrower wells. The interface is the place where the strongest electron–phonon interaction took place. Thus, it leads to the decrease of the G factor. But, the tendency on the decrease of the G factor does not hold for extremely small $q_{\parallel}$. As the well gets narrower, the increasing of the G factor has been canceled out by the decreasing of the H factor and results in the weak dependence for well width narrower than 4 nm. This behavior was not found in the earlier calculated results[24] where the assumption of an infinite quantum well was made.

For the $S-$ mode, due to the small H factor, the scattering rate is much smaller than the rate of the $S+$ mode. In addition, the increased H factor with the well width compensates the decreased G factor each other. This results in a weak dependence of scattering rates on the well width.

The scattering rate of the confined mode increases from 0.27 to 2.2 ps^{-1} while the rate of the half-space mode decreases sharply from 0.13 to 0.12 ns^{-1} as the well width is increased from 2 to 12 nm. The increase of the scattering rate of the confined mode is due to the increased G factor as the well width is increased. On the contrary, the G factor decreases for the half-space mode.

There is a crossover point of the scattering rate for the confined mode and the $S+$ mode at a well width of 10 nm and an Al composition of 0.3. So the confined mode is the major relaxation channel for hot electrons in wide quantum wells and the $S+$ mode is responsible for the narrow wells. Although the total scattering rate only varies slightly with the well width, there still can be a strong dependence[25] of the AELR on the well width when the phonon energy of the corresponding modes is considered.

IV. CONCLUSION

In conclusion, the dependence of electron-optical phonon interaction in GaAs/$Al_xGa_{1-x}As$ quantum wells on the Al composition and the well width is studied numerically based on the DCM model. The scattering rate of the symmetric interface mode shows a stronger dependence on the Al composition than that of the confined mode. The $S-$ mode has the strongest dependence on the Al composition due to the H factor. The effective phonon energy was estimated and

compared with the earlier experimental results. The dependence on the Al composition is in reasonable agreement with the experimental results. The difference between the calculated result and the experimental result is attributed to the simplified average phonon energy in $Al_xGa_{1-x}As$ alloy used in the calculation. Strong dependence of the scattering rate on the well width for the $S+$ and the confined mode suggests the importance of the well width on the hot carrier relaxation via polar optical phonon scattering. The DCM model in the electron–phonon interaction is more accurate than the bulk and bulklike phonon models.

ACKNOWLEDGMENT

This work is supported by the National Science Council under Grant No. NSC89-2218-E009-055.

[1] C. H. Yang, J. M. Carlson-Swindle, S. A. Lyon, and J. M. Worlock, Phys. Rev. Lett. **55**, 2359 (1985).
[2] R. G. Ulbrich, Phys. Rev. B **8**, 5719 (1973).
[3] S. J. Manion, M. Artaki, M. A. Emanuel, J. J. Coleman, and K. Hess, Phys. Rev. B **35**, 9203 (1987).
[4] R. Fuchs and K. L. Kliewer, Phys. Rev. A **140**, 2076 (1965).
[5] J. J. Licari and R. Evrard, Phys. Rev. B **15**, 2254 (1977).
[6] N. Mori and T. Ando, Phys. Rev. B **40**, 6175 (1989).
[7] R. Chen, D. L. Lin, and T. F. George, Phys. Rev. B **41**, 1435 (1990).
[8] K. Huang and B. Zhu, Phys. Rev. B **38**, 13 377 (1988).
[9] A. K. Sood, J. Menendez, M. Cardona, and K. Ploog, Phys. Rev. Lett. **54**, 2111 (1985).
[10] A. K. Sood, J. Menendez, M. Cardona, and K. Ploog, Phys. Rev. Lett. **54**, 2115 (1985).
[11] A. Seilmeier, H. J. Hubner, G. Abstreiter, G. Weimann, and W. Schlapp, Phys. Rev. Lett. **59**, 1345 (1987).
[12] J. K. Jain and S. Das Sarma, Phys. Rev. Lett. **62**, 2305 (1989).
[13] K. Leo, W. W. Ruhle, and K. Ploog, Phys. Rev. B **38**, 1947 (1988).
[14] K. Leo, W. W. Ruhle, H. J. Queisser, and K. Ploog, Phys. Rev. B **37**, 7121 (1988).
[15] H. Lobentanzer, W. Stolz, J. Nagle, and K. Ploog, Phys. Rev. B **39**, 5234 (1989).
[16] J. Shah, A. Pinczuk, A. C. Gossard, and W. Wiegmann, Phys. Rev. Lett. **54**, 2045 (1985).
[17] G. Fasol, W. Hackenberg, H. P. Hughes, K. Ploog, E. Bauser, and H. Kano, Phys. Rev. B **41**, 1461 (1990).
[18] D. N. Mirlin, B. P. Zakharchenya, I. I. Reshina, A. V. Rodina, V. F. Sapega, A. A. Sirenko, V. M. Ustinov, A. E. Zhukov, and A. Y. Egorov, Semiconductors **30**, 377 (1996).
[19] V. F. Sapega, M. P. Chamberlain, T. Ruf, M. Cardona, D. N. Mirlin, K. Totemeyer, A. Fischer, and K. Eberl, Phys. Rev. B **52**, 14 144 (1995).
[20] K. W. Sun, H. Y. Chang, C. M. Wang, T. S. Song, S. Y. Wang, and C. P. Lee, Solid State Commun. **115**, 563 (2000).
[21] S. Adachi, J. Appl. Phys. **58**, R1 (1985).
[22] T. Ando, A. B. Fowler, and F. Stern, Rev. Mod. Phys. **54**, 437 (1982).
[23] T. Thoai and H. Haug, Phys. Status Solidi B **98**, 581 (1980).
[24] S. Rudin and T. L. Reinecke, Phys. Rev. B **41**, 7713 (1990).
[25] H. C. Lee, C. P. Lee, and K. W. Sun, Abstracts of the Tenth International Conference on Phonon Scattering in Condensed Matter (Hanover, 2001), p. 178.